Lattice dynamics and elasticity in thermoelectric $Mg_2Si_{1-x}Sn_x$

Benedikt Klobes*
University of Applied Sciences Bremerhaven, An der Karlstadt 8, 27568 Bremerhaven, Germany and Jülich Centre for Neutron Science JCNS and Peter Grünberg Institute PGI, JARA-FIT, Forschungszentrum Jülich GmbH, 52425 Jülich, Germany

Johannes de Boor
Institute of Materials Research, German Aerospace Center, Linder Höhe, 51147 Köln, Germany.

Ahmet Alatas† and Michael Y. Hu
Advanced Photon Source, Argonne National Laboratory, Argonne, Illinois 60439, USA

Ronnie E. Simon
Jülich Centre for Neutron Science JCNS and Peter Grünberg Institute PGI, JARA-FIT, Forschungszentrum Jülich GmbH, 52425 Jülich, Germany

Raphaël P. Hermann‡
Materials Science and Technology Division, Oak Ridge National Laboratory, Oak Ridge, Tennessee 37831, USA

Lattice dynamics and elastic constants in $Mg_2Si_{1-x}Sn_x$ were investigated using resonant ultrasound spectroscopy, Mössbauer spectroscopy, nuclear inelastic scattering and inelastic X-ray scattering. Increasing the Sn content x results in smaller elastic constants, lower Sn specific Debye temperature, lower speed of sound, and a softening of acoustic Sn specific phonons. However close to band convergence at about $x = 0.6$, the shear modulus is well below the expected value, which suggests a pronounced connection between band convergence and lattice dynamics in this system. Based on the determined speed of sound and average phonon group velocity, the importance of optical phonons for lattice thermal conductivity is discussed, as the significant reduction in both velocities would yield an implausibly low lattice thermal conductivity of only about 70% of the experimental value. Sn specific thermodynamic quantities calculated from the Sn specific density of phonon states substantiate the general softening of lattice vibrations upon substitution of Si by Sn. A major contribution to the vibrational entropy is thus due to Sn specific vibrational modes. The generalized density of phonon states in $Mg_2Si_{1-x}Sn_x$ derived from inelastic X-ray scattering for one composition shows that vibrational modes related to lightweight Mg and Si set in above 12.5 meV, whereas Sn specific modes are concentrated around 11 meV.

I. INTRODUCTION

Thermoelectric energy generation has attracted considerable attention in the past decades. On the one hand, thermoelectrics may play a vital role in increasing energy efficiency by harvesting waste heat and, on the other hand, thermoelectric materials display interesting and interconnected physical properties and phenomena. The thermoelectric figure-of-merit $ZT = \frac{S^2\sigma}{\kappa_e+\kappa_l}$, where S is the Seebeck coefficient, σ is the electrical conductivity, and κ_e and κ_l are the electronic and lattice contributions to thermal conductivity[1], illustrates that a good thermoelectric material must accommodate potentially conflicting transport properties. But besides exhibiting a high ZT value in a broad temperature range, the ideal thermoelectric material should also be made of inexpensive, abundant and non-toxic elements, in order to facilitate wide-spread and environmentally compatible application.

Solid solutions based on Mg_2Si and Mg_2Sn certainly fulfill the latter requirements and exhibit favorable ZT values above 1[2,3] competitive with PbTe based thermoelectrics and skutterudites, not least due to their low mass density. Within the $Mg_2Si_{1-x}Sn_x$ solid solution system, highest figures-of-merit have been found for stoichiometries around $Mg_2Si_{0.4}Sn_{0.6}$ due to high $S\sigma^2$ values and favorable thermal conductivites[2,4–6]. *Ab-initio* calculations showed[2,7] that close to $x = 0.6$ two low-lying electronic bands associated with different effective electron mass converge, which results in an overall increase in effective electron mass and, consequently, of Seebeck coefficient. Moreover, thermal conductivity is reduced upon isovalent substitution of Si by Sn presumably due to phonon scattering by mass and strain fluctuations. Lattice dynamics in $Mg_2Si_{1-x}Sn_x$, which eventually form the microscopic basis for the lattice contribution to thermal conductivity, were investigated in detail for the end members Mg_2Si and Mg_2Sn. Both experimental and theoretical densities of phonon states, phonon dispersions and elastic constants were derived[8–12] and mostly agree on an overall softening of phonon energies and elastic constants upon Si substitution by Sn. For $Mg_2Si_{1-x}Sn_x$ solid solutions, predominantly theoretical investigations were published[13–15] with the recent exception of neutron scattering results for $x = 0.25,\ 0.5,\ 0.75$[16]. The general, potentially simplifying picture emerging from these findings is that lattice dynamics in $Mg_2Si_{1-x}Sn_x$ can be

roughly understood in a Vegard's law picture[16,17]. However, lattice dynamics and elasticity close to electronic band convergence at $x = 0.6$ is still rather uncharted territory, although the general importance of band convergence and structure for the development of new thermoelectrics is well recognized[18,19].

Here, we aim to investigate elastic constants and (Sn specific) lattice dynamics particularly of samples close to composition $x = 0.6$ using resonant ultrasound spectroscopy, Mössbauer spectroscopy, nuclear inelastic scattering and inelastic X-ray scattering. The shear modulus C_{44} is found to be significantly lower in samples close to band convergence than expected within an average (Vegard's law) model, which is further substantiated by acoustic Sn specific phonon modes. The theoretically expected splitting of (Mg,Si) and Sn related phonons in high and low energy regions[13], respectively, can be corroborated. Moreover, the rather low average phonon group velocity in this system substantiates the notion of a significant contribution of optical phonons to thermal conductivity.

II. MATERIAL AND EXPERIMENTAL DETAILS

All samples (see Tab. I for stoichiometries) were synthesized by induction melting followed by crushing and compaction by current assisted sintering[20]. Because for thermoelectric applications the charge carrier concentration of ternary $Mg_2Si_{1-x}Sn_x$ needs to be optimized samples were actually n-doped by small additions of Sb or Bi. Microstructural analysis as well as thermoelectric transport data for sample $Mg_2Si_{0.79}Sn_{0.2}Sb_{0.01}$ can be found in Ref.[21] and for the other three samples in Ref.[22]. Room temperature X-ray diffraction (XRD) measurements were carried out using a Huber powder diffractometer with Cu $K_{\alpha 1}$ radiation in combination with an image plate Guinier detector. Lattice parameters and phase content were analyzed using the software JANA2006[23].

Mössbauer spectra were obtained on a constant-acceleration spectrometer using a 10 mCi $Ca^{119m}SnO_3$ for ^{119}Sn Mössbauer spectroscopy. The velocity calibration was performed with α-Fe at room temperature utilizing a ^{57}Co/Rh source. All Mössbauer spectra discussed herein were obtained using powder samples and isomer shifts are reported with reference to the source. The significant γ-background due to fluorescence of the ^{119}Sn Mössbauer source was suppressed using a 50 μm thick Pd foil placed between source and sample.

Room temperature (polycrystalline) elastic constants C_{11} and C_{44} were derived from resonant ultrasound spectroscopy (RUS)[24] measurements using parallelepiped shaped, polycrystalline samples of about 2 mm^3 each. Using the RPR code[25], C_{11} and C_{44} were calculated from the first 20 resonances.

Nuclear inelastic scattering (NIS) experiments[26], which are based on phonon assisted absorption of synchrotron radiation by an appropriate Mössbauer resonance (the 23.88 keV resonance of ^{119}Sn in the present case), were performed at sector 30-ID of the Advanced Photon Source using a high-resolution monochromator with an energy resolution of 1 meV[27]. Measurements were carried out at room temperature as determined by the principle of detailed balance. Sn specific densities of phonon states (DOS) were extracted from NIS spectra using the Fourier-Log decomposition as implemented in the software DOS[28].

For sample $Mg_2Si_{0.39}Sn_{0.6}Bi_{0.01}$, a room temperature, inelastic X-ray scattering (IXS) experiment was carried out at sector 30-ID of the Advanced Photon Source using an incident energy of 23.73 keV obtained by a high resolution monochromator[27] and using high resolution analyzers[29]. IXS spectra were recorded for seven different analyzer positions with an average scattering vector of $Q_{av} = 6.047$Å^{-1}. Individual IXS spectra were weighted and summed and the resulting spectrum was further analyzed using the Fourier-Log decomposition procedure aforementioned and assuming a hypothetical recoil energy calculated from sample stoichiometry (similar to the approach outlined in Ref.[30]). The resulting generalized density of phonon states thus contains contributions from each element weighted by the respective IXS cross-section.

III. RESULTS AND DISCUSSION

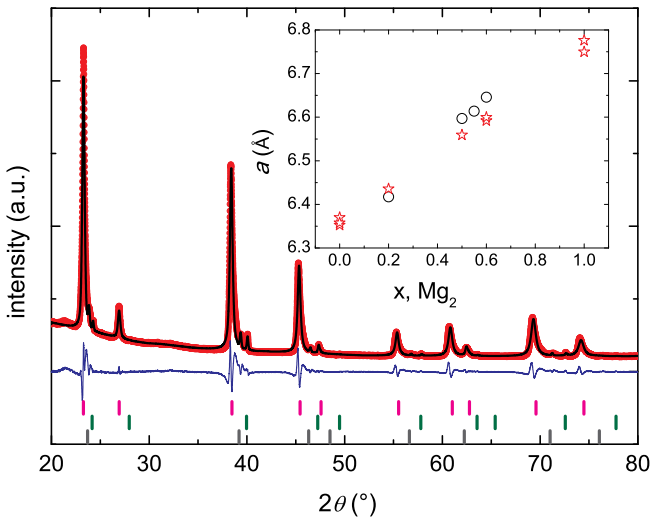

FIG. 1. Representative X-ray diffraction pattern for the $Mg_2Si_{1-x}Sn_x$ samples. In this case, $Mg_2Si_{0.39}Sn_{0.6}Bi_{0.01}$, there are two minor impurity phases present. Ticks (top to bottom) represent the major $Mg_2Si_{1-x}Sn_x$ phase (magenta), Mg_2Si (green) and β-Sn (dark green). The inset shows the lattice parameter, a, as a function of the nominal Sn content of the major phase for each sample (circles). Literature data for different compositions (red stars) are from Refs.[31–35].

A representative XRD pattern is shown in Fig. 1 and exhibits contributions from three different phases. Be-

side the major solid solution $Mg_2Si_{1-x}Sn_x$, antifluorite Mg_2Si and tetragonal β-Sn can be detected in two of the four samples (see Tab. I). Concerning the lattice parameter a, the major phase is reasonably close to Vegard's law in each case (see inset to Fig. 1), although the actual Sn content of the major phases might slightly deviate from the nominal composition. Thus, the sample sequence in terms of Sn content is still represented by the nominal composition. The occurrence of impurity phases, in particular a Si-rich and a Sn-rich phase, is often observed for the $Mg_2Si_{1-x}Sn_x$ system[21,22]. This is due to a miscibility gap between Mg_2Si and Mg_2Sn, whose borders are the subject of controversial discussion[36–38]. Moreover, synthesis kinetics can also affect the presence of impurity phases[22]. However, the general single-phase

sample	phase	a (Å)	I
$Mg_2Si_{0.79}Sn_{0.2}Sb_{0.01}$	I	6.4173(1)	1.00
$Mg_2Si_{0.49}Sn_{0.5}Bi_{0.01}$	I	6.5969(1)	1.00
$Mg_2Si_{0.44}Sn_{0.55}Bi_{0.01}$	I	6.6138(1)	0.967(1)
	II	6.3794(4)	0.012(1)
	III	6.4809(3)	0.021(1)
$Mg_2Si_{0.39}Sn_{0.6}Bi_{0.01}$	I	6.6460(1)	0.970(1)
	II	6.3810(4)	0.004(1)
	III	6.4899(4)	0.026(1)

TABLE I. Lattice parameter a, and relative contribution I, obtained by XRD analysis for the solid solutions $Mg_2Si_{1-x}Sn_x$ (I) and impurity phases Mg_2Si (II) and β-Sn (III).

character of all samples is supported by Mössbauer spectroscopy (see Fig. 2 for representative spectra), as in all cases spectra could be well modeled using a single Lorentzian absorption line. Isomer shifts δ are weakly temperature dependent and increase from about 1.8 to 1.9 mm/s with decreasing temperature, which is in good agreement with literature on binary Mg_2Sn[39], whereas Mössbauer linewidths are virtually constant at about 0.9(1) mm/s. Room temperature isomer shifts with respect to unit cell volume, V_{cell}, are shown in the inset to Fig. 2. Notably, slightly larger isomer shifts can be observed for those $Mg_2Si_{1-x}Sn_x$ compounds with high Sn content, *i.e.* with increased unit cell volume. Assuming that V_{cell} and electron density at the ^{119}Sn nucleus site are inversely proportional, the increase of δ with increasing V_{cell} is unexpected[40] and points towards a change of bonding character or bonding mechanism.

Temperature dependent Mössbauer spectroscopy measurements were used in order to determine the Lamb-Mössbauer factor f_{LM} of each sample within a Deybe model[41] (see Fig. 3). The corresponding Sn specific Debye temperatures decrease with increasing Sn content and are well below calculated general Debye temperatures[12] indicating overall softer Sn than Mg or Si phonons.

Room temperature elastic constants C_{11} and C_{44} determined using RUS are shown in Fig. 4. Both elastic constants continuously decrease with increasing Sn content, which is expected considering the much lower elastic constants of Mg_2Sn compared to Mg_2Si[8,9]. However upon approaching the Sn content associated with electronic band convergence, the absolute values of the elastic constants decrease rapidly and the shear modulus C_{44} is well below expected values for Sn contents ≥ 0.5. Transversal, v_T, longitudinal, v_L, and average (Debye) speed of sound v_S were calculated according to $v_{L,T} = \sqrt{C_{11,44}/\rho}$ and $3v_S^{-3} = 2v_T^{-3} + v_L^{-3}$[42], where ρ is the mass density, and are shown in the inset to Fig. 4. In general, the decrease in elastic moduli and the speed of sound with increasing Sn content is in line with the decreasing (Sn specific) Debye temperatures as observed by Mössbauer spectroscopy. Moreover, the notable decrease of shear modulus C_{44} might point towards an electronic

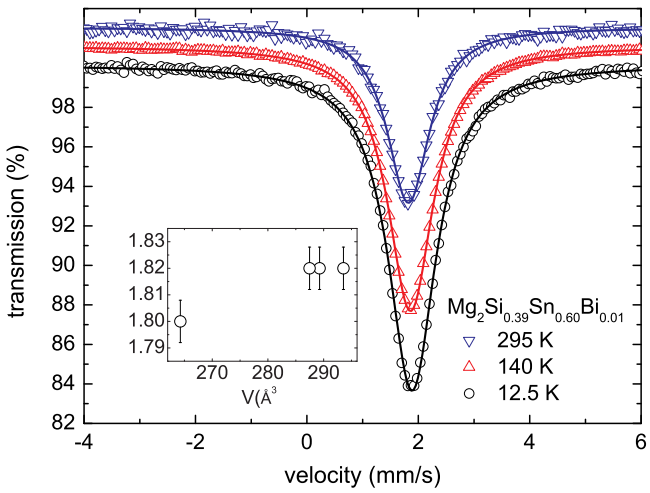

FIG. 2. Representative ^{119}Sn Mössbauer spectra at different temperatures used to calculate Lamb-Mössbauer factors (see Fig. 3). The inset shows room temperature isomer shifts, δ, with respect to the corresponding unit cell volume, V.

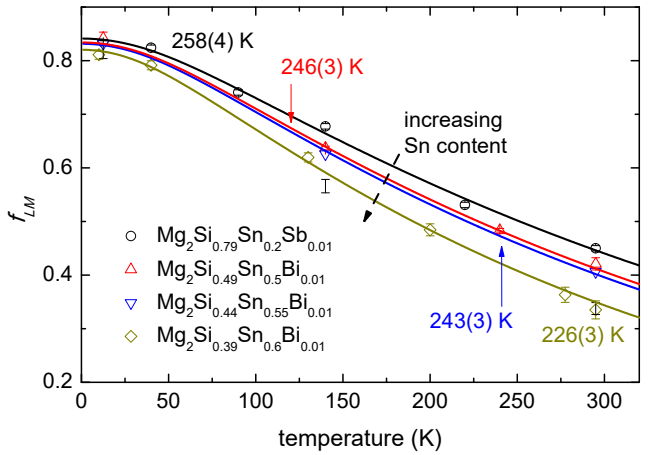

FIG. 3. Lamb-Mössbauer factors f_{LM} obtained from temperature dependent Mössbauer measurements within a Debye model (solid lines) and corresponding Debye temperatures θ_D.

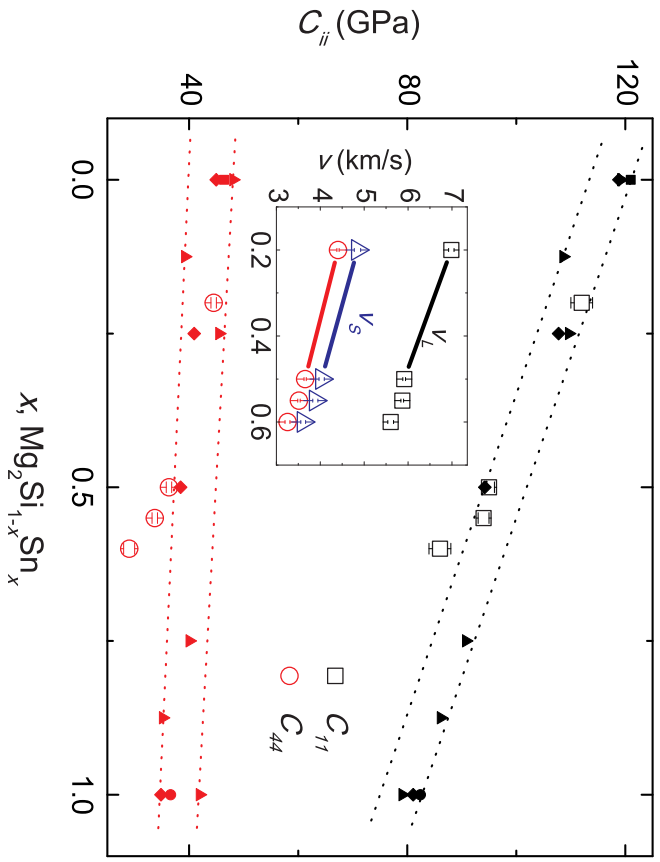

FIG. 4. Elastic moduli C_{11} and C_{44} extracted from room temperature resonant ultrasound spectroscopy (open symbols) for different $Mg_2Si_{1-x}Sn_x$. Full symbols mark literature data: experimental data for Mg_2Si (square) and Mg_2Sn (circle) from Refs.[8,9] and theoretical calculations for $Mg_2Si_{1-x}Sn_x$ (triangle from Ref.[13] and diamond from Ref.[14]). The dashed lines are guides for the eye. The inset depicts the longitudinal, v_l, transversal, v_t, and average v_s speed of sound calculated using C_{11} and C_{44} (see text for further details). Error bars are well below the size of the data points.

band structure effect on elastic constants due to electronic band convergence. As all samples exhibit similar ratios of physical/measured density vs. X-ray/theoretical density, potential effects of density variations on the measurement of elastic constants can be excluded.

Sn specific densities of phonon states (DOS) were obtained from NIS experiments and are shown in Fig. 5. All DOS are dominated by a peak around 11 meV and exhibit rather broad features at higher energies. The phonon cutoff was determined to be 32.5 meV in all cases. This agrees with theoretical DOS available for Sn contens below 0.25 and above 0.75[13]. However, the experimentally determined spectral weight of modes with energy above 16 meV is found to be slightly more pronounced than expected theoretically. The Sn specific DOS in $Mg_2Si_{0.39}Sn_{0.6}Bi_{0.01}$ and $Mg_2Si_{0.49}Sn_{0.5}Bi_{0.01}$ are almost indistinguishable, whereas there is a significant stiffening of low energy acoustic modes in $Mg_2Si_{0.79}Sn_{0.2}Sb_{0.01}$

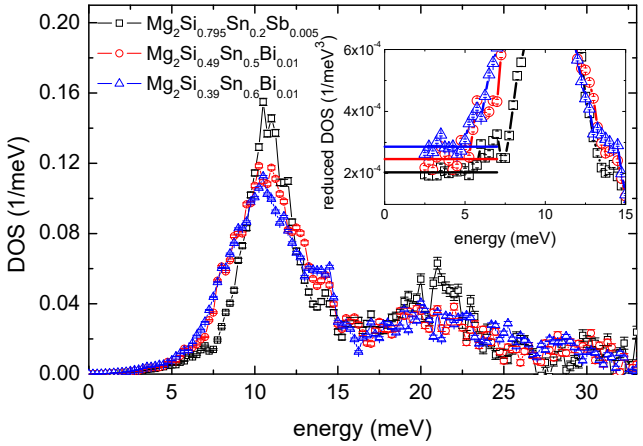

FIG. 5. Sn specific densities of phonon states obtained from NIS measurements at room temperature. The inset shows the low energy part of the reduced densities of phonon states including the corresponding Debye levels (horizontal lines).

which is accompanied by an overall narrowing of the first spectral peak. This is in agreement with the elastic contants, which increase with decreasing Sn content, and with ab-initio calculations[13]. These calculations show a similar redistribution of Sn specific phonon modes to lower energies in the acoustic region with increasing Sn content x for ternary $Mg_2Si_{1-x}Sn_x$. This is also a strong indication that the change of dopant (from Sb to Bi in the present case) likely has a negligible effect on the Sn specific DOS. Thus, the $Mg_2Si_{1-x}Sn_x$ lattice stiffens with an increasing number of Mg-Si bonds.

Based on these DOS, several Sn specific thermodynamic quantities can be calculated, *e.g.*, the Lamb-Mössbauer factor f_{LM}, the vibrational entropy S_{vib} and the mean force constant $\overline{F}$[28]. These quantities are summarized in Tab. II. The trend of decreasing Lamb-Mössbauer factor with increasing Sn content is consistent with conventional Mössbauer spectroscopy results. Notably, Lamb-Mössbauer factors calculated from DOS are slightly lower than the ones calculated within a Debye model (see Fig. 3 and compare Tab. II), but agree within their respective errors. As force constants mostly depend on the spectral weight of high frequency modes, it is not surprising that all Sn specific force constants agree within their error bars. However, Sn specific force constants are higher than the Si and Ge specific force constants in Mg_2Si and Mg_2Ge, respectively[11]. The temperature dependence of the vibrational entropy was calculated for some compositions[13], which allows one to estimate a vibrational entropy of 3.21 k_B/atom for $Mg_2Si_{0.79}Sn_{0.2}Sb_{0.01}$ and 3.61 k_B/atom for $Mg_2Si_{0.44}Sn_{0.55}Bi_{0.01}$ and $Mg_2Si_{0.39}Sn_{0.6}Bi_{0.01}$. Thus, the Sn specific vibrational entropy of 4.66(2) k_B/atom for $Mg_2Si_{0.79}Sn_{0.2}Sb_{0.01}$ is higher than the average contribution of Mg and Si due to the high concentration of spectral weight of low phonon energies.

The low energy limit of the DOS divided by energy

squared, $L_D = \lim_{E\to 0}[g(E)/E^2]$, where $g(E)/E^2$ is the so-called reduced DOS, can be used to calculate[43] the average phonon group velocity $v_{NIS} = \sqrt[3]{m/(2\pi^2\hbar^3\overline{m}nL_D)}$, where m is the mass of the nuclear resonant nucleus (the mass of Sn-119 in the present case), $\overline{m}$ is the average mass in the unit cell, and n is the atomic density. For the calculation of v_{NIS}, the Debye level was estimated from the almost constant reduced DOS in the energy interval 2.5 meV $\leq E \leq$ 5 meV (see inset to Fig. 5). As data below 2.5 meV is potentially affected by the subtraction procedure of elastic scattering, it was omitted for estimating L_D. Calculated average phonon group velocities v_{NIS} are compared to v_S calculated from elastic constants in Tab. II. The average phonon group velocity and the speed of sound exhibit the same general trend, i.e., a decrease with increasing Sn content. For $Mg_2Si_{0.44}Sn_{0.55}Bi_{0.01}$ and $Mg_2Si_{0.39}Sn_{0.6}Bi_{0.01}$, v_{NIS} and v_S are quite close and agree within their error bars, whereas v_{NIS} is significantly lower than v_S for $Mg_2Si_{0.79}Sn_{0.2}Sb_{0.01}$. It is possible that the subtraction of the elastic contribution was insufficient in this case, which might affect the Debye level determination. On the other hand, the average phonon group velocity of phonons with energies in the interval between 2.5 and 5 meV does not necessarily coincide with the speed of sound, i.e., with the average group velocity of phonons with $E \to 0$. Such differences between speed of sound and average phonon group velocity determined for phonon energies of a few meV were observed for other compounds[44,45] and cannot be ruled out for $Mg_2Si_{0.79}Sn_{0.2}Sb_{0.01}$. However, the reason of this discrepancy cannot be unambiguously solved.

In binary Mg_2X (X = C, Si, Ge, Sn, Pb), the average phonon group velocity in the low energy limit, *i.e.*, the speed of sound, is considered to be the most important parameter for understanding lattice thermal conductivity[46]. Extending this notion to the solid solution $Mg_2Si_{1-x}Sn_x$ and considering $\kappa_l = \frac{1}{3}Cv_S^2\tau$, where C is the specific heat, τ is the phonon relaxation time, and potential phonon energy dependencies have been neglected, for the calculation of the lattice thermal conductivity, a significant decrease of κ_l is expected based on v_S and v_{NIS} determined from RUS and NIS, respectively. This expectation also persists, if a more elaborate Callaway model[47] including phonon scattering by solute atoms[48,49] is used, which yields[50] κ_l = 1.53 $Wm^{-1}K^{-1}$ for $Mg_2Si_{0.49}Sn_{0.5}Bi_{0.01}$ and κ_l = 1.36 $Wm^{-1}K^{-1}$ for $Mg_2Si_{0.39}Sn_{0.6}Bi_{0.01}$. These values account only for about 60 % of the lattice thermal conductivities experimentally determined of these samples[22] and of theoretically calculated κ_l[17,51]. However, ab-initio calculations have shown that optical phonons, which are not taken into account by the Callaway model, may contribute significantly to lattice thermal conductivity in $Mg_2Si_{1-x}Sn_x$[15] due to their significant dispersion. Indeed, the theoretical estimate of the optical phonon contribution closely matches the discrepancy of 40 % between actual lattice thermal conductivity and the Callaway model calculation based on mass contrast scattering presented herein. Additionally introducing Umklapp scattering further reduces the calculated[52] lattice thermal conductivity by about one order of magnitude. The deviation from experimental values thus increases, which again illustrates that lattice thermal conductivity in this system cannot be understood solely based on acoustic phonons. Thus, the notion that optical phonon modes contribute significantly to κ_l in this system is supported experimentally.

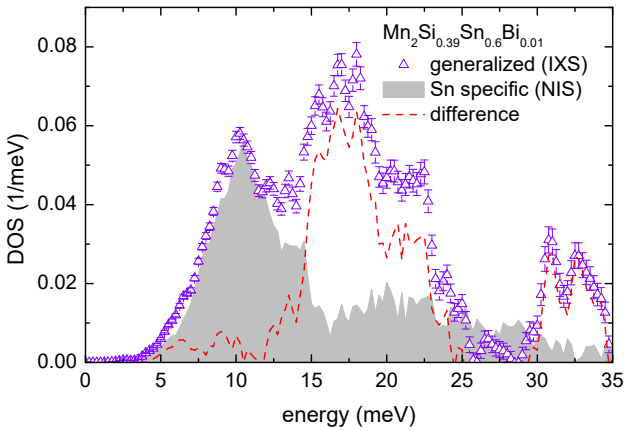

FIG. 6. Generalized density of phonon states in $Mg_2Si_{0.39}Sn_{0.6}Bi_{0.01}$ obtained from IXS. The Sn specific DOS in this sample is also shown. As the IXS signal contains contributions from all elements in the sample, the Sn specific contribution was scaled according to its expected contribution using the atomic form factor and the atomic mass of Sn.[53] The difference between IXS and NIS related DOS is depicted by the dashed line and represents (Mg,Si) related phonons.

The generalized DOS in $Mg_2Si_{0.39}Sn_{0.6}Bi_{0.01}$ obtained from IXS spectra is shown in Fig. 6 together with the appropriately scaled Sn specific DOS obtained from NIS. Sn specific phonon modes contribute about 50% to the generalized DOS due to the high atomic number of Sn as compared to Mg and Si. Phonon modes below 15 meV are almost exclusively associated to Sn, whereas Mg and Si contribute predominantly to modes between 15 and 25 meV as well as above 30 meV. In general, this separation between Sn and (Mg,Si) related modes can be expected considering the atomic masses and shows similar features as DOS calculations for high and low Sn contents[13]. A similar gap between Sn and Mg specific phonon energies was also observed by neutron scattering experiments combined with density functional theory calculations[16]. Moreover, the phonon cutoff at about 35 meV is in good agreement with theoretical results for the close composition $Mg_2Si_{0.5}Sn_{0.5}$[16].

IV. CONCLUSIONS

Elastic constants and lattice dynamics in $Mg_2Si_{1-x}Sn_x$ were investigated using RUS, Mössbauer spectroscopy, nuclear inelastic scattering by the ^{121}Sn Mössbauer resonance and inelastic X-ray scattering. In general, the lattice is found to soften upon Si substitution by Sn, which is reflected by a decrease of the elastic constants C_{11} and C_{44}, which also entails a decrease of the speed of sound, by a softening of Sn partial acoustic phonons and by lower Sn specific Debye temperatures obtained from Mössbauer spectroscopy. The shear modulus C_{44} decreases significantly close to band convergence and exhibits unexpected low values. This is also reflected by the calculated speed of sound, which is in good agreement with the average phonon group velocity derived from NIS. The drop of the shear modulus close to band convergence suggests a close connection between electronic and vibrational properties for such compositions, which opens the more general question about the potential connection between band convergence and lattice dynamics. The comparison between the Sn specific DOS and the generalized DOS obtained by means of IXS exemplifies that Sn and (Mg,Si) related phonons are well separated in terms of energy in $Mg_2Si_{1-x}Sn_x$ with Sn mostly taking part in vibrational modes below 15 meV. This also entails that Sn specific vibrations strongly contribute to the overall vibrational entropy. The unexpectedly low speed of sound and average phonon group velocity in $Mg_2Si_{1-x}Sn_x$ close to band convergence results in an implausibly low lattice thermal conductivity within a simple Callaway model. Thus, the importance of optical phonons, which are not taken into account by the latter model, for thermal transport in $Mg_2Si_{1-x}Sn_x$ as pointed out theoretically[15,51] is experimentally substantiated. It remains an open question, whether certain optical modes predominantly contribute to lattice thermal conductivity or all optical modes are comparably relevant. In any case, ways to reduce the optical contribution should be explored for improving the thermoelectric figure-of-merit of this system.

ACKNOWLEDGMENTS

NIS and IXS measurements (RPH) supported by the U.S. Department of Energy, Office of Science, Basic Energy Sciences, Materials Sciences and Engineering Division. This research used resources of the Advanced Photon Source, a U.S. Department of Energy (DOE) Office of Science User Facility operated for the DOE Office of Science by Argonne National Laboratory under Contract No. DE-AC02-06CH11357. Financial support by the German Research Society (DFG) within the framework of priority program SPP 1386 is acknowledged. JDB acknowledges endorsement by the Helmholtz Association of German Research Centers.

* bklobes@hs-bremerhaven.de

[1] H. J. Goldsmid, *Introduction to Thermoelectricity* (Springer-Verlag, 2009).
[2] W. Liu, X. Tan, K. Yin, H. Liu, X. Tang, J. Shi, Q. Zhang, and C. Uher, Phys. Rev. Lett. **108**, 166601 (2012).
[3] A. U. Khan, N. Vlachos, and T. Kyratsi, Scripta Mater. **69**, 606 (2013).
[4] X. Zhang, Q.-m. Lu, L. Wang, F.-p. Zhang, and J.-x. Zhang, J. Electron. Mater. **39**, 1413 (2010).
[5] P. Gao, I. Berkun, R. D. Schmidt, M. F. Luzenski, X. Lu, P. Bordon Sarac, E. D. Case, and T. P. Hogan, J. Electron. Mater. **43**, 1790 (2014).
[6] J.-H. Bahk, Z. Bian, and A. Shakouri, Phys. Rev. B **89**, 075204 (2014).
[7] X. J. Tan, W. Liu, H. J. Liu, J. Shi, X. F. Tang, and C. Uher, Phys. Rev. B **85**, 205212 (2012).
[8] W. B. Whitten, P. L. Chung, and G. C. Danielson, J. Phys. Chem. Solids **26**, 49 (1965).
[9] L. C. Davis, W. B. Whitten, and G. C. Danielson, J. Phys. Chem. Solids **28**, 439 (1967).
[10] P. Baranek, J. Schamps, and I. Noiret, J. Phys. Chem. B **101**, 9147 (1997).
[11] D. Bessas, R. E. Simon, K. Friese, M. Koza, and R. P. Hermann, J. Phys. Condens. Matter **26**, 485401 (2014).
[12] X. Liu, Y. Wang, J. O. Sofo, T. Zhu, L.-Q. Chen, and X. Zhao, J. Mater. Res. **30**, 2578 (2015).
[13] H. Peng, C. Wang, J. Li, H. Wang, Y. Sun, and Q. Zheng, Solid State Commun. **152**, 821 (2012).

[14] L. Na-Na, S. Ren-Bo, and D. Da-Wei, Chinese Phys. B **18**, 1979 (2009).
[15] X. J. Tan, G. Q. Liu, H. Z. Shao, J. T. Xu, B. Yu, H. C. Jiang, and J. Jiang, Appl. Phys. Lett. **110**, 143903 (2017).
[16] L. Chaput, J. Bourgeois, A. Prytuliak, M. M. Koza, and H. Scherrer, Phys. Rev. B **91**, 064304 (2015).
[17] P. Bellanger, S. Gorsse, G. Bernard-Granger, C. Navone, A. Redjaimia, and S. Vives, Acta Mater. **95**, 102 (2015).
[18] Y. Pei, X. Shi, A. LaLonde, H. Wang, L. Chen, and G. J. Snyder, Nature **473**, 66 (2011).
[19] J. Zhang, L. Song, S. H. Pedersen, H. Yin, L. T. Hung, and B. B. Iversen, Nat. Commun. **8**, 13901 (2017).
[20] T. Dasgupta, C. Stiewe, R. Hassdorf, A. J. Zhou, L. Boettcher, and E. Müller, Phys. Rev. B **83**, 235207 (2011).
[21] J. de Boor, S. Gupta, H. Kolb, T. Dasgupta, and E. Müller, J. Mater. Chem. C **3**, 10467 (2015).
[22] T. Dasgupta, C. Stiewe, J. de Boor, and E. Müller, Phys. Status Solidi A **211**, 1250 (2014).
[23] V. Petricek, M. Dusek, and L. Palatinus, "Jana2006," (2006), Institute of Physics, Praha, Czech Republic.
[24] A. Migliori and J. L. Sarrao, *Resonant Ultrasound Spectroscopy: Applications to Physics, Materials Measurements, and Nondestructive Evaluation*, 1st ed. (Wiley-Interscience, 1997).
[25] A. Migliori, Rev. Sci. Inst. **76**, 121301 (2005).
[26] R. Röhlsberger, *Nuclear Condensed Matter Physics with Synchrotron Radiation* (Springer-Verlag, Berlin, 2004).
[27] T. S. Toellner, A. Alatas, and A. H. Said, J. Synchrotron Radiat. **18**, 605 (2011).
[28] V. Kohn and A. Chumakov, Hyperfine Interact. **125**, 205 (2000).
[29] A. H. Said, H. Sinn, and R. Divan, J. Synchrotron Radiat. **18**, 492 (2011).
[30] A. Bosak and M. Krisch, Phys. Rev. B **72**, 224305 (2005).
[31] W. Klemm and H. Westlinning, Z. Anorg. Allg. Chem. **245**, 365 (1941).
[32] R. Saravanan and M. C. Robert, J. Alloys Compd. **479**, 26 (2009).
[33] M. Kubouchi, K. Hayashi, and Y. Miyazaki, J. Alloys Compd. **617**, 389 (2014).
[34] Q. Zhang, J. He, T. J. Zhu, S. N. Zhang, X. B. Zhao, and T. M. Tritt, Appl. Phys. Lett. **93**, 102109 (2008).
[35] W. Luo, M. Yang, F. Chen, Q. Shen, H. Jiang, and L. Zhang, Mat. Sci. Eng. B **157**, 96 (2009).
[36] S. F. Muntyanu, E. B. Sokolov, and E. S. Makarov, Zh. Neorgan. Mater. **2**, 870 (1966).
[37] A. Kozlov, J. Grobner, and R. Schmid-Fetzer, J. Alloys Compd. **509**, 3326 (2011).
[38] J. Bourgeois, J. Tobola, B. Wiendlocha, L. Chaput, P. Zwolenski, D. Berthebaud, Q. Recour, F. Gascoin, and H. Scherrer, Funct. Mater. Lett. **6**, 1340005 (2013).
[39] J. E. Inglesfield, J. Phys. Chem. Solids , 1443 (1970).
[40] P. E. Lippens, Phys. Rev. B **60**, 4576 (1999).
[41] P. Gütlich, E. Bill, and A. X. Trautwein, *Mössbauer Spectroscopy and Transition Metal Chemistry* (Springer Berlin Heidelberg, Berlin, Heidelberg, 2011).
[42] O. L. Anderson, J. Phys. Chem. Solids **24**, 909 (1963).
[43] M. Y. Hu, W. Sturhahn, T. S. Toellner, P. D. Mannheim, D. E. Brown, J. Zhao, and E. E. Alp, Phys. Rev. B **67**, 094304 (2003).
[44] B. Klobes, M. Herlitschke, K. Z. Rushchanskii, H.-C. Wille, T. T. A. Lummen, P. H. M. van Loosdrecht, A. A. Nugroho, and R. P. Hermann, Phys. Rev. B **92** (2015).
[45] M. Herlitschke, B. Klobes, I. Sergueev, P. Hering, J. Persson, and R. P. Hermann, Phys. Rev. B **93** (2016).
[46] A. Chernatynskiy and S. R. Phillpot, Phys. Rev. B **92** (2015).
[47] J. Callaway, Phys. Rev. **113**, 1046 (1959).
[48] P. G. Klemens, Phys. Rev. **119**, 507 (1960).
[49] B. Abeles, Phys. Rev. **131**, 1906 (1963).
[50] For the calculation of κ_l within a Callaway model including mass contrast scattering, Debye temperatures were linearly interpolated from calculated values[12] according to sample stoichiometry and the phonon relaxation time due to scattering by solute atoms was calculated also according to sample stoichiometry following Ref.[49].
[51] W. Li, L. Lindsay, D. A. Broido, D. A. Stewart, and N. Mingo, Phys. Rev. B **86**, 174307 (2012).
[52] Umklapp scattering was taken into account following the example given by Ref.[54]. For all samples, the Gruneisen parameter $\gamma = 1.2$ of Mg_2Si was assumed[11]. This represents a lower limit to the contribution of Umklapp scattering within a Callaway model, as γ of Mg_2Sn was calculated to be 1.61[12].
[53] N. Yazdani, T. Nguyen-Thanh, M. Yarema, W. M. M. Lin, R. Gao, O. Yarema, A. Bosak, and V. Wood, J. Phys. Chem. Lett. **9**, 1561 (2018).
[54] H. Wang, T. Wang, J. Hwang, W. Su, H. Kim, J. Zhai, X. Wang, C. Wang, and W. Kim, Inorg. Chem. Front. **5**, 793 (2018).

sample	f_{LM}	$f_{LM,MB}$	S_{vib} (k_B/atom)	$\overline{F}$ (N/m)	v_{NIS} (m/s)	v_S (m/s)
$Mg_2Si_{0.79}Sn_{0.2}Sb_{0.01}$	0.40(2)	0.44(3)	4.66(2)	124(10)	4310(60)	4830(80)
$Mg_2Si_{0.44}Sn_{0.55}Bi_{0.01}$	0.36(2)	0.40(3)	4.80(1)	118(6)	3750(70)	3880(70)
$Mg_2Si_{0.39}Sn_{0.6}Bi_{0.01}$	0.35(1)	0.36(3)	4.78(1)	123(4)	3530(60)	3610(70)

TABLE II. Lamb-Mössbauer factor f_{LM}, vibrational entropy S_{vib}, and mean force constant $\overline{F}$ calculated from Sn specific DOS measured at room temperature. The Lamb-Mössbauer factor $f_{LM,MB}$ obtained by applying a Debye model to conventional Mössbauer spectroscopy results (see Fig. 3), the average speed of sound v_S calculated from elastic constants, and the phonon group velocity v_{NIS} calculated from Sn specific DOS are also shown for comparison.